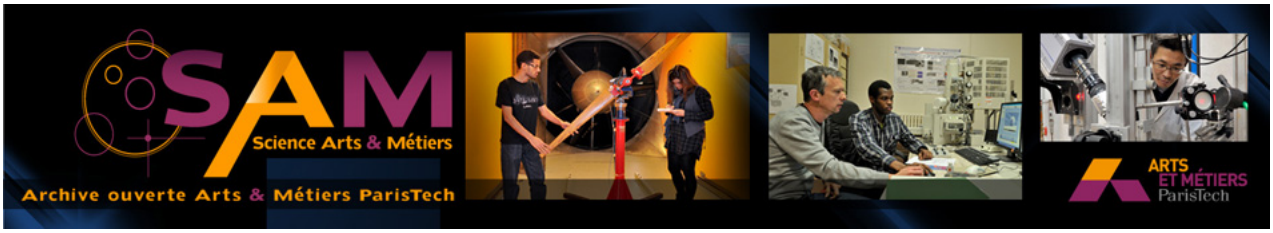

Reflection on the Measurement and Use of the Topography of the Indentation Imprint

J. Marteau, M. Bigerelle, S. Bouvier, and A. Iost

Laboratoire Roberval, UMR 7337, Université de Technologie de Compiègne, Centre de Recherches de Royallieu, Compiègne Cedex, France

Summary: The goal of this paper is to study the main uses of the residual imprint of the indentation test. It also discusses the different technologies and methods employed in this context. The difficulties encountered when trying to exploit the full potentials of the imprint are thoroughly examined. A survey of the literature on the quantification of the pile-up clearly shows that there is a lack of consensus on the measurement of the residual imprint as well as on treatment methods. Therefore, in order to widen the application fields of the indentation residual imprint, relevant and standardized indicators should be established.

Key words: indentation residual imprint, morphology, pile-up, topography

Introduction

The indentation test, whether conventional or instrumented, is particularly valued for several reasons: its convenience, the requirement of only small amounts of materials, as well as the test's ability to determine the properties of materials that, due to their configuration, could not be identified with other conventional tests. However, the test results remain difficult to interpret (Giannakopoulos *et al*., '94), and their reliability (Schneider *et al*., '99) is still under discussion.

A survey of the literature on the residual indentation imprint identified three main uses for the test. The first is dedicated to the measurement of the contact area. It aims at checking the results or the validity of the hypotheses made for the calculation of the hardness or Young's modulus, using instrumented indentation data. The second purpose concerns the characterization of the behavior of the material being tested. As an example, the orientation and shape of cracks initiated during the test are correlated with material parameters. The emergence of pile-up or sink-in, which is, respectively, an upward or inward flow of the material, also contributes in understanding the material's behavior. The third purpose of the test is the use of the imprint in finite element or molecular dynamics simulations, as described below.

Despite these common purposes, there is a lack of consensus on the measurement and treatment methods used for the study of the imprint indentation. There are several measurement means: some studies are primarily focused on the use of optical microscopy (Yang *et al*., 2006), scanning electron microscopy (SEM) (Dwyer-Joyce *et al*., '98), or confocal microscopy (Santos *et al*., '98; Keryvin, 2007), while others are based on profile measurement (Hainsworth *et al*., '98), atomic force microscopy (AFM) measurements (Yang *et al*., 2008) or interferometric microscopy (Su *et al*., 2012; Marteau *et al*., 2013). It is worth noting that most of the studies rely on qualitative information. Several others try to observe the evolution of some topographic parameters in order to fully exploit the information given by the topography of the residual indentation print.

The complexity in data interpretation and the need for a better understanding of the material behavior underneath the indenter motivated the present work, i.e. the study of the use of the residual indentation imprint. The paper is divided into three main parts. The first section is devoted to the presentation of the indenter shapes and the measurement methods. In the second section, the main uses of the residual indentation imprint are described in detail. The third section deals with the key parameters used in studying pile-up behavior and emphasizes the lack of standardization of morphological indicators and of a prevailing technique for the study of

Address for reprints: J. Marteau, Laboratoire Roberval, UMR 7337, Universitè de Technologie de Compiègne, Centre de Recherches de Royallieu, BP 20529, 60205 Compiègne Cedex, France
E-mail: julie.marteau@utc.fr

indentation impressions. The main difficulties that can be encountered in a quantitative estimation of the indentation imprint are also discussed.

Indenter Shapes and Measurement Methods

Indenter Shapes

There are several types of indenter tips that can be distinguished by their scale of use. At the macro-scale, three indenters are used: Vickers, Rockwell, and Brinell. For use at the microscale and sub-microscale levels, the following indenters are commonly used:

- Vickers,
- Berkovich (three-sided pyramid having the same contact area as the Vickers indenter),
- Knoop,
- Spherical,
- Cube-corner, and
- Conical.

At the nanoscale level, the Berkovich and cube-corner tips are usually preferred. This is principally due to the difficulty of getting a perfectly four-sided indenter (i.e., Vickers, Knoop) or a surface of revolution (i.e., spherical or conical indenters). The main indenter shapes are schematized in Figure 1.

Measurement Methods

There are predominantly six different measurement methods used to examine the indentation imprints: optical microscopy, SEM, confocal microscopy, interferometry, tactile profilometry, and AFM. These measurement techniques have different advantages and disadvantages. In this section, only some tips are depicted, in order to give a global idea of the use of these different methods.

If the surface cannot be touched because it is too soft (risk of scratch) or too stiff, then all the techniques introduced in the previous paragraph can be used, except tactile profilometry or AFM in contact mode.

Optical microscopy is particularly convenient for surface observation. It offers rapid image acquisition, both at the macro- and micro-scales. For higher resolution, SEM is more suitable but that method remains time-consuming.

For three-dimensional observations, AFM, interferometric microscopy, confocal microscopy, or tactile profilometry can be used. The selection of a technique depends on the indenter shape and the scale of the imprint. Tactile profilometry can be used for three-dimensional observations but is not a rapid procedure. It should only be used to draw the profile of an imprint (e.g., for the bisectors of a Berkovich imprint). Usually, tips having a diameter from 1 to 10 μm are used for the measurements, thus offering a small resolution in contrast to AFM.

The interferometric and confocal microscope observations offer a good depth of field but only at higher magnifications. Higher magnification is thus recommended for the observation of imprints having sharp angles (e.g., cube-corner indent). AFM offers a better resolution compared to the previous techniques. Therefore, the AFM technique is more suitable when accurate inspections of the topography of the imprint are required. However, AFM is a very time-consuming process and can only be used for small scales (i.e., areas smaller than 100×100 μm). It is worth mentioning that the AFM tip should be carefully monitored in order to avoid any deterioration of the results.

Main Uses of the Indentation Imprint

Validation of Hypotheses and Explanation of the Indentation Results

One of the most recurrent uses of the indentation residual imprint is the validation of the experimental results. For example, it can be used in order to understand special features in the load-versus-indentation depth curves or to check the value of material characteristics (elastic modulus, hardness) that are calculated when using the indentation test.

The study of the shape of the imprint also provides valuable help to understand the evolution of the

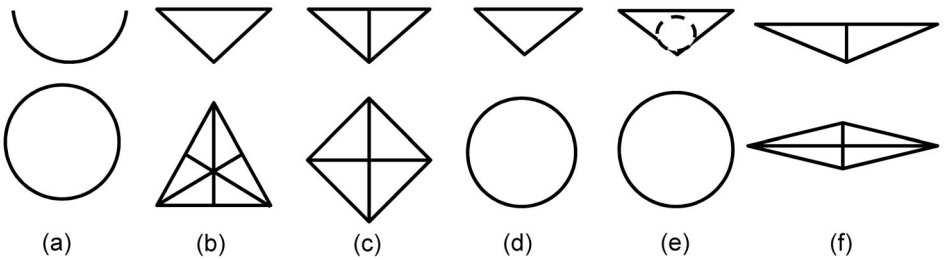

Fig. 1. Different shapes of indenters: (a) Spherical, (b) Berkovich, (c) Vickers, (d) Conical, (e) Rockwell, (f) Knoop.

recorded loading curve. Such analysis can explain the origin of phenomena such as pop-in, which is an abrupt step in the recording of the curve. Barnoush *et al*. (2010) studied the pop-in phenomenon by combining different techniques. The information given by the residual imprint permitted qualification of the behavior of material, through the observation of pile-up occurrences. The use of the electron channeling contrast imaging technique enabled observations about the dislocation substructure. Combining these results with the load-versus-indentation depth curves revealed that the occurrence of pop-in was directly linked with the subsurface dislocation structure in aluminum. Beegan *et al*. (2004) also studied the origin of the appearance of pop-in in carbon nitride and copper films. That study showed that the pop-in occurrence was associated with a fracture of the film. It was evidenced using AFM imaging of the indents. Chen *et al*. (2010) investigated the relationship between pop-in and shear band appearance through imprint inspection.

The residual imprint can also be used to localize the indentation, if the material has two or more phases (Göken and Kempf, '99; Arpat and Ürgen, 2011).

The measurement of the imprint contributes to confirming or refuting the assumptions used for the calculation of the contact area. Indeed, the errors introduced into the estimation of the contact area can lead to an inaccurate assessment of the Young's modulus and of the hardness. Several sources of errors can be listed. Among them, (i) the tilting of the sample due to a non-planar surface (Kashani and Madhavan, 2011); (ii) the occurrence of sink-in or pile-up (Farges and Degout, '89; Ou *et al*., 2008) around the indent, as shown in Figure 2. In this later situation, the use of the (Oliver and Pharr, '92) method for materials experiencing pile-up can lead to an underestimation of the contact area. This underestimation results from an erroneous identification of the region supporting the load. Indeed, as indicated by Chaudhri and Winter ('88), the pile-up area also supports the indenter load. Thus, the material behavior should be carefully observed (Constantinides *et al*., 2006). When pile-up is known to be important, or if the indent is not symmetrical, Fischer-Cripps (2006) advised to directly measure the contact area but gave no details on the measurement method. For example, Beegan *et al*. (2005) and Charleux *et al*. (2008) used AFM measurements to determine the true contact area (and thus the true hardness) because of pile-up occurrence.

Finally, the residual imprint contributes to assessing the consistency of the hardness results. Youn and Kang (2006) used the residual imprint to understand the difference of hardness among heat-treated squeeze-cast alloy. The use of AFM demonstrated that there was a difference of shape, distribution, and size of the silicon particles dispersed in the eutectic matrix, as well as a height difference between the phases. The latter decreased with the increase of the age hardening time. This variation was the cause for the disparity of hardness in the specimens. Bolelli *et al*. (2008) examined the origin of the low values of plasma-sprayed TiO_2 through the observation of the cross-section of the indent and found that sub-surface cracking disturbed the calculation of the material hardness.

Material Characterization

Due to the complexity of the developed stresses, the indentation test provides a valuable source of information on the material properties. A wide variety of instances are given in the published papers. As an example, Frick *et al*. (2005) used AFM measurements of the residual indentation depth before and after heating shape-memory alloys to quantify their recovery capabilities.

Different features of the residual indentation imprint can be used to characterize the materials. Some studies are based on the investigation of the pile-up patterns to try to improve understanding about material behavior,

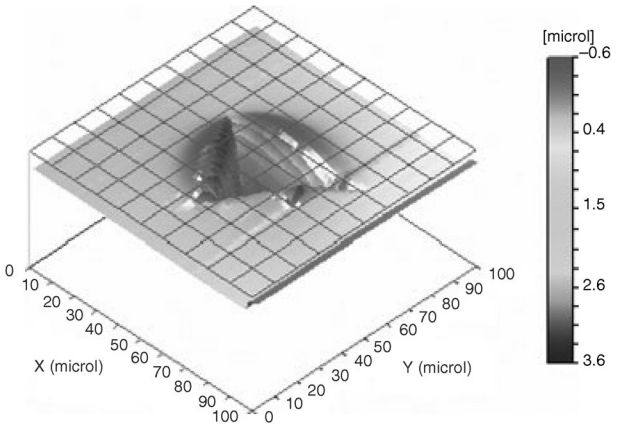

Fig. 2. NanoVision image of KMPR residual imprint. Pile-up can be observed.

while others are focused on crack growth or the appearance of slip patterns.

The tendency of a material to pile-up or sink-in is often used in order to characterize its behavior. Howell *et al*. (2008) compared the behavior of four silicate reference glasses by quantifying the amount of pile-up as indentation depth increased. The amount of pile-up was determined by using AFM representative line scans of the bisector of the triangular indents. The pile-up amount was then defined as the height above the surface divided by the maximum indentation depth, multiplied by 100. Similarly, Das *et al*. (2005) used the differences in pile-up amounts to propose a classification of materials into three main categories. The first category gathered materials showing piling-up. The second was dedicated to materials undergoing sinking-in, and the last category to materials experiencing cracking. Woodcock and Bahr (2000) examined the plastic zone evolution taking place at the specimen surface with a focus on the variation of the geometry of the indenter and the chosen length scale during indentation. Results showed that an indicator based on the quantification of the plastic zone area provided a more robust method of assessing a material's response to plastic deformation at very fine scales than the traditional use of hardness.

Other published works used the residual indentation imprint for investigation about material behavior. Such studies observed and tried to explain the pattern of the plastic zone and its evolution as a function of loading or crystal orientation. Zong and Soboyejo (2005) linked the pile-up shapes of face-centered cubic single crystals with their orientation. However, these findings still need to be completed, since no relationships between the pile-up shape and the activated slip systems were proposed. On the other hand, Elban and Armstrong ('98) managed to explain the impression shapes in single crystal ammonium perchlorate, by identifying the slip systems and crack planes activated during the indentation test.

Other studies examined cross-sections of residual imprints to attempt to observe the physical phenomena taking place under the indent. Demir *et al*. (2009) studied the link between indentation size effect and geometrically necessary dislocations through the detection of backscattered electrons.

Finally, material behaviors can be analyzed through the examination of crack development, to aid understanding about the fracture mechanisms induced by contact. This kind of analysis usually requires a cross-section of the indent and then observation of the obtained surface, using SEM or transmission electron microscopy (TEM), as in the work by Carvalho and De Hosson (2006). Formulae have also been developed to calculate fracture toughness by measuring the length of the surface cracks produced by indentation (Bhattacharya *et al*., 2009). Links between the material composition and its behavior under indentation can also be investigated by analysis of the angles of subsurface cracks. Bertoldi and Sglavo (2004) showed that, depending on the glass composition, the angles of cracks observed on the cross-section of the indent were different.

Residual Imprint and Simulations

The employment of residual imprints is also valuable in molecular dynamics or finite element simulations of the indentation test. Two main uses can be identified: the assessment of the indentation simulation results and the exploitation of the imprint profile in inverse methods (i.e., for identification of material parameters).

The use of the residual imprint can help to check several types of hypotheses such as the validity of the behavior law. Gadelrab *et al*. (2012) compared the indent profiles obtained with the Drucker-Prager model and the elastic-perfectly plastic behavior with experimental measurements made with AFM. The value of the friction coefficient is assessed by superimposing experimental cross-section profiles with simulation results. By comparing the height of the pile-ups, Karthik *et al*. (2012) confirmed the choice of 0.2 for the Coulomb friction coefficient.

Su and Anand (2006) compared the contours plots of the equivalent plastic shear strain after unloading with the corresponding micrograph of the cross-section displaying shear-band patterns. For a better comparison, both results were superimposed. To validate the numerical modeling, Wang *et al*. (2008) compared the simulated pile-up pattern with experimental AFM results that had been published by Barshilia and Rajam (2002) and Huang *et al*. (2005).

SEM images of the indentation imprints are also used to evaluate the ability of developed models to predict the crack front profiles, as recently proposed by Chen *et al*. (2011).

The second use of the residual imprint in numerical simulation is linked to the development of inverse approaches. When the indentation test is performed using a geometrically similar indenter (i.e., conical, pyramidal), it is well known that a unique set of mechanical properties cannot be found using a single load-versus-displacement curve (e.g., Chen *et al*., 2007). In order to overcome such limitations, several research groups (e.g., Casals and Alcalá, 2005; Lee *et al*., 2009) built a methodology for extracting the yield strength, Young's modulus, strain-hardening exponent, and hardness from indentation experiments, using the residual indentation imprint to select between different sets of identified material parameters. Bolzon *et al*. (2004) built a new inverse approach combining data from load-versus-displacement curves and from the indentation imprint. The indentation imprint was described using the vertical displacements of simulated points, which were taken at equally spaced positions in

order to reproduce AFM measurements. This process considerably enriched the method and enabled more accurate and robust results. However, the approach was only based on simulated data, i.e. the numerical results were not compared with experimental ones.

This first section shows that, even if the residual indentation imprint has three predominant uses, the methods and measurements employed remain very different. This point is further discussed in the following section.

Quantitative Information

Example: Pile-Up Quantification

Through a study of the pile-up quantification in the literature, this section will give evidence that there is lack of uniformity on the building of indicators.

Blunt and Sullivan ('94) have proposed one of the first methods to accurately quantify the extent of pile-up. A method was presented that progressively truncated three-dimensional area maps in order to quantify the pile-up volumes. In other methods, length or height measurements were compared. Mordehai *et al*. (2011) measured maximum height of the pile-up to understand the development of the deformation. In order to evaluate the height evolution, the film height, prior to indentation, was considered as the reference. On the other hand, Zhou *et al*. (2008) defined the pile-up height by subtracting the contact height from the total height of the imprint. As shown in these first two examples, the selected reference for the measurement of the pile-up height is not unique and varies among different research groups.

Some authors focused analysis on the evolution of the pile-up as a function of the indentation depth. Bellemare *et al*. (2007) proposed a ratio in which the pile-up height is divided by the residual indentation depth, i.e. the maximum height over the maximum depth of the indent. This ratio is used by several authors (e.g., Choi *et al*., 2008; Huang *et al*., 2010).

In other papers, the pile-up is quantified through an in-plane measurement of its extent (Cabibbo and Ricci, 2012). Zhang *et al*. (2011) focused the comparison on the geometries of the indentation, quantitatively measured by defining a ratio between two parameters, using a profile of the cross-section of the imprint. The numerator represented the distance including the pile-up and the indentation width, while the denominator was the range of indentation without pile-up. Beegan *et al*. (2005) used AFM images to calculate both the plastic area and the volume, including the piled-up material. It was assumed that the pile-up formed an arc of a radius r at the indent edge, as shown in Figure 3.

A final method rests on the estimation of the deformation through the measurement of the radius of the pile-up. Woodcock and Bahr (2000) used such a method to evaluate the relationship between the plastic zone size and the contact radius. To do so, a section was drawn along the major axis of each pile-up lobe, and the lobe radii were measured by analyzing the AFM measurement results with image software. The estimated radii were averaged to obtain the mean maximum extent of plastic deformation. Similarly, Zong and Soboyejo (2005) used the pile-up radius to study the evolution of the deformation as a function of the indentation depth.

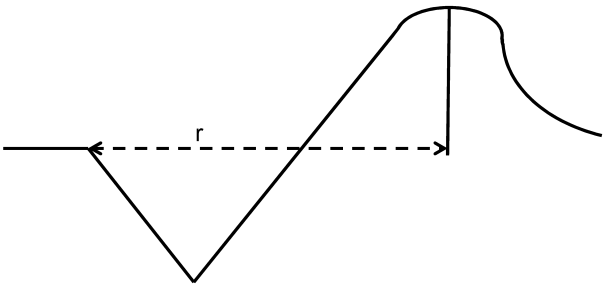

Fig. 3. Cross-section showing the definition of r, the radius of the pile-up.

Overall, the literature review clearly highlights the absence of specific and standardized approaches for pile-up quantification.

A dominant Technique?

It is worth noting that a review of a large number of published papers indicates that there is a lack of supremacy of an experimental technique for the examination of the residual imprint. The selected method seems to be guided by the targeted application. As an example, the assessment of the simulation results requires a method that provides the pattern of the deformation around the residual indent. That pattern can then be compared with the out-of-plane displacement, calculated with the finite element simulation. Liu *et al*. (2008) carried out nanoindentation tests on single-crystal copper having different orientations. The computed out-of-plane displacements were compared with AFM images of the indent imprints. Instead of using the cross-section of the imprint, the focus was on the measurement of the plastic zone around the indent, with only a qualitative description given of the symmetry of the pile-up distribution. Eidel (2011) qualitatively evaluated the difference between the calculated pile-up topography and the experimental one by using SEM images, although that research also focused on the comparison of the pile-up symmetries. Hence, SEM and AFM images can thus be chosen for the same purpose. Contrary to the SEM, it should be noted that the AFM gives a quantitative estimation of the out-of-plane displacements. However, as in most papers,

this quantitative information remains unused by the researchers. Alcalá *et al*. (2008) also used SEM images in order to compare the simulated residual imprint morphology with experimental measurements, in order to assess whether the simulated imprint shapes could be reproduced for an arbitrary distribution of grain orientations.

While the literature on the topic is abundant, there is no objective evaluation of the advantages and disadvantages of the different experimental techniques, except in select cases. An *et al*. (2011) showed that the SEM gave better results than the AFM when studying the deformation mechanisms and fracture behavior of TiN coating on a Si (111) substrate. It was found that the AFM measurements could give an erroneous estimation of the diameter of the interfacial fracture between the coating and the substrate. Indeed, the blister measured with the AFM did not correspond to the diameter of the interfacial fracture.

Carefully comparing the range of application of the measurement techniques, it is evident that their accuracy and advantages will probably help to significantly expand the use of the residual imprint test.

Difficulties

Despite the lack of uniformity of the measurements and methods, some difficulties are common. Among the problems is the selection of an appropriate reference, in order to share a common scale between the different measurements of the residual indents. Bellemare *et al*. (2007) determined the pile-up height and the residual indentation depth after linearly interpolating the original position of the surface obtained from profilometry. In order to ensure that the area chosen as the original surface position was not affected by the deformation, points were selected that were at a distance of four times the residual radius of contact from the centre of the indent. Similarly, Stelmashenko *et al*. ('93) determined a zero-level plane corresponding to the undisturbed surface around the indentation, using a least square method. Arivuoli *et al*. (2000) chose to subtract the AFM profile measured before the indentation to the one measured after the indentation. That process enabled the calculation of the real pile-up, by removing the influence of surface roughness. The determination of the surface reference position is a key point when dealing with the measurement of the topography of the imprint. However, this reference and its determination may change from one measurement technique to another.

Roughness is also a common difficulty when dealing with profile measurements (e.g., Randall *et al*., '96). Some studies underlined the difficulty in localizing the indent impression when the experiments were carried out on rough surfaces (e.g., Babu and Kang, 2010). Others attempted to overcome the problem by increasing the load at which the material is studied. Barshilia and Rajam (2002) chose a load of 25 mN for the AFM investigation. Difficulties arose in assessing the pile-up formation at 7 mN, because it was of the same order of magnitude as the roughness (average roughness of 30–40 nm). Similarly, Kese *et al*. (2005) failed in finding the pile-up height at low loads. For higher loads, that height was estimated as the upper point of the distinctly formed ridge. The latter changed to a plateau for lower loads. Thus, the contact perimeter was defined as the point of departure of a tangent parallel to the face of the pile-up.

Another difficulty arises when the deformation around the indent is not symmetric. For the sake of simplicity, only one profile is measured through an indent. For instance, Jee and Lee (2010) compared the response of different polymers using the indentation profiles. A line parallel to the baseline of the triangle and crossing the deepest point was considered. Then, the profiles obtained for all the studied polymers were superimposed. Top-view AFM images were also shown, but no comments were made on the symmetry of the deformation around the indents. On the other hand, Beegan *et al*. (2003) measured profiles of the Berkovich residual impression by sweeping the indent AFM image perpendicular to the edge of the triangle to the opposite corner, for each edge of the triangle. However, no treatment was made to attempt to overlay the obtained profiles in order to compare them. Similarly, Navamathavan *et al*. (2006) drew three profiles across a Vickers indent impression, showing the irregular shape of the indent, due to material pile-up occurring at only one side of the pyramidal indent. Zhou *et al*. (2008) also emphasized the fact that, for the studied material, pile-up only occurred at the indent edge of the Berkovich imprint and not at the corners of the triangle.

The estimations of perimeters, areas, or volumes are still current issues in topographic measurements because they are scale-dependent (Brown and Siegmann, 2001; Cantor and Brown, 2009). Thus, the determination of the relationships between pile-up appearance and work hardening requires the choice of an appropriate scale.

As indicated in the previous sections, the imprint could give valuable information about material behavior. However, its characterization raises several questions: What is the best way to determine the reference of a surface? How is the roughness effect to be treated? Is the measurement of one profile enough to describe the behavior of a material? What profiles would be selected when a lack of symmetry occurs? Several answers can be given and will need to be assessed. For instance, for the indent profiles, some may use only one profile of the imprint, even if it does not perfectly fit the experimental reality. Others may try to build some averaging technique or a statistical method that may better represent the experimental reality. Similar approaches

TABLE I Comprehensive overview

Refs.	Technique	Device reference	Z range	Z Resolution	Scale	Material	Indenter type	Application	Aim
Alcalá *et al.* (2008)	Micrograph	—	—	—	—	Well-annealed polycrystalline copper	Vickers	Simulation	To compare experimental and simulation results
An *et al.* (2011)	SEM	JEOL JSM-6700F	—	—	$d_{max} = 5$ μm	TiN coating on a Si (111) substrate	Cube corner	Coating	To study crack development
	AFM	—	—	—	$d_{max} = 5$ μm	TiN coating on a Si (111) substrate	Cube corner	Coating	To measure pile-up height and the diameter of the interfacial fracture
Arivuoli *et al.* (2000)	Profilometer	—	—	—	$d \approx 5$ μm	GaAs/InP heterostructures grown by metal organic vapor phase epitaxy	Trigonal diamond pyramid with an equilateral triangular cross-section and a 90° angle between each face and the opposing edge	Coating	To measure "pile-up" effects
	AFM	—	—	—	$d \approx 5$ μm	GaAs/InP heterostructures grown by metal organic vapor phase epitaxy	Trigonal diamond pyramid	Coating	To confirm pile-up
Arpat and Ürgen (2011)	SEM	JEOL 5410 SEM and JEOL JSM-7000F FE-SEM	—	—	$d_{max} \approx 5$ μm	Cu-Al intermetallics	Vickers	Phase	To localize the indentation impressions into the studied phases
Babu and Kang (2010)	AFM	—	—	—	$d_{max} \approx 3$ μm	Al-based hybrid composites containing graphite nanofiber/ alumina short fiber	Berkovich	MMCs	Pile-up observation
Barnoush *et al.* (2010)	AFM	—	—	—	$d_{max} \approx 1.5$ μm	High purity aluminum	Berkovich	Pop-in	Pile-up observation
Barshilia and Rajam (2002)	AFM	—	2–3 μm	<1 nm	$d_{max} \approx 5$ μm	Cu/Ni multilayer coatings	Berkovich	Coatings	Pile-up shape is observed
Beegan *et al.* (2003)	AFM	Surface Probe Microscope Topometrix Explorer	10 μm	3–10 nm	$d_{max} \approx 9$ μm	Copper films on oxidised Si substrates	Berkovich	Coatings	To calculate the total projected contact area to determine the film hardness. To determine the extent and nature of the pile-up found around indents
Beegan *et al.* (2004)	AFM	Surface Probe Microscope Topometrix Explorer	10 μm	3–10 nm	$d_{max} \approx 5$ μm	Carbon nitride and copper films deposited on silicon substrates	Berkovich	Coatings	To observe pile-up and cracking occurrence
Beegan *et al.* (2005)	AFM	Surface Probe Microscope Topometrix Explorer	10 μm	3–10 nm	$d_{max} \approx 5$ μm	Sputter deposited copper films on oxidised Si substrates	Berkovich	Coatings	To observe if pile-up occurs and to calculate the corresponding volume
Bellemare *et al.* (2007)	Profilometer	Tencor P10	—	—	Order of magnitude: μm	Pure nickel with different grain sizes	Conical	Pile-up	To measure pile-up height
Bertoldi and Sglavo (2004)	SEM and optical	—	—	—	$d_{max} \approx 150$ μm	Soda-borosilicate glass	Vickers	Cracks	To observe the geometry of the cracks
Bhattacharya *et al.* (2009)	SEM	FEI Quanta 200 FEG SEM	—	—	$d_{max} \approx 9$ μm	Silicon particles in Al-18.5wt %Si alloys	Vickers	Cracks	To measure the crack length to calculate fracture toughness
	TEM	JEOL 2010F and Philips CM12	—	—	—	Silicon particles in Al-18.5wt %Si alloys	Vickers	Cracks	To investigate indentation-induced subsurface damage and fracture features
	Profilometer	WYKO NT 1100	—	—	$d_{max} \approx 9$ μm	Silicon particles in Al-18.5wt %Si alloys	Vickers	Cracks	To measure pile-up. Coupled with SEM, statistical analysis of the frequency of subsurface lateral
Blunt and Sullivan ('94)	Profilometer	Designed and built in-house	—	—	$d \approx 0.4$ mm	70:30 brass	Vickers	Pile-up	To calculate the volume of the surface disturbance
Bolelli *et al.* (2008)	SEM (with FIB)	XL-30, FEI	—	—	$d_{max} \approx 40$ μm	Plasma-sprayed TiO_2 on grit-blasted C40 steel plates.	Vickers and Berkovich	Cracks	To study sub-surface cracking
Cabibbo and Ricci (2012)	Nanoindenter Scanning Probe Mode	Hysitron© UBI-1	—	—	$d \approx 5$ μm	DHP-copper in both H58 and annealed conditions	Berkovich	Pile-up	To measure the real contact area
Carvalho and De Hosson (2006)	SEM	Philips-XL30(s)-FEG	—	—	$d_{max} \approx 6$ μm	TiN/(Ti,Al)N multilayer coatings onto steel substrates	Berkovich	Cracks	Observation of the cross-section of the indents to examine the fracture mechanisms
	TEM	JEOL 2010 4000 EX/II and JEOL 2010 FEG	—	—	$d_{max} \approx 6$ μm	TiN/(Ti,Al)N multilayer coatings onto steel substrates	Berkovich	Cracks	Observation of the cross-section of the indents to examine the fracture mechanisms
Casals and Alcalá (2005)	Optical	—	—	—	—	Al 2098-T8 alloy	Berkovich	Simulation	Methodology of identification of properties gives two sets. Pile-up observation helps choosing

Continued

TABLE I Continued

Refs.	Technique	Device reference	Z range	Z Resolution	Scale	Material	Indenter type	Application	Aim
Charleux *et al.* (2008)	AFM	Veeco Dimension3000	—	—	$d_{max} \approx 10$ μm	Amorphous, partially and totally crystallized Vitreloy1 samples	Berkovich	Pile-up	E and H are estimated using the value of the contact area derived from AFM imaging
Chaudhri and Winter ('88)	Optical	—	—	—	$d_{max} \approx 3$ mm	Work-hardened mild steel and annealed/work-hardened copper	Vickers and conical indenters	Pile-up	To show that the pile-up region also supports the indenter load
Chen *et al.* (2010)	SEM and TEM	FEI, G^2 20 S-Twin TEM	—	—	$d_{max} \approx 100$ μm	Bulk metallic glasses	Vickers	Shear-bands	To observe shear band spacing
	AFM	—	—	—	$d_{max} \approx 100$ μm	Bulk metallic glasses	Vickers	Shear-bands	To obtain the topography of shear band circles
Chen *et al.* (2011)	SEM	—	—	—	Wedge lengths = 4.06 μm and 7.24 μm	Continuous black diamond films deposited on top of silicon substrates	Wedge indentation	Cracks	To compare the experimental crack front profiles with the simulation results
Choi *et al.* (2008)	Profilometer	KLA-Tencor P-10	—	—	$d_{max} \approx 20$ μm	Ni-W alloys (nanocystalline alloys)	Berkovich	Simulation/Pile-up	To measure the residual indentation depth, the pile-up height. To study the influence of the plastic gradient upon pile-up height
Constantinides *et al.* (2006)	AFM	—	—	—	$d_{max} \approx 0.4$ mm	Ti-TiB-TiB2 specimen	Berkovich	Pile-up	To demonstrate that there is no significant pile-up
Das *et al.* (2005)	SEM and optical	—	—	—	$d_{max} \approx 700$ μm	Various engineering materials (steels, brass, pure copper, pure aluminum, nickel base super alloy)	Ball indentation	Pile-up	To study the extent of pile-up
Demir *et al.* (2009)	SEM (EBSD)	—	—	—	$d_{max} \approx 5$ μm	Cu single crystal	Conical indenter with a spherical tip	Density of GNDs	To calculate GND density under the indent
Dwyer-Joyce *et al.* ('98)	SEM	—	—	—	$d_{max} \approx 40$ μm	PET with and without magnetic layers	Berkovich	Illustration	To show residual impression
Eidel (2011)	SEM	JEOL and Hitachi S520a	—	—	$d_{max} \approx 60$ μm	FFC single crystal made of a Ni-base superalloy	Vickers and spherical indentation	Simulation	To compare experimental and simulation results
Elban and Armstrong ('98)	Optical	—	—	—	$d_{max} \approx 100$ μm	Single crystal ammonium perchlorate	Vickers	Cracks	To observe the impression shapes and the cracks
Farges and Degout ('89)	3D rugosity apparatus	Built at E.C.T.A.	—	—	$d \approx 50$ μm	Steels, copper, thick hard chromium and PVD titanium nitride film	Vickers	Pile-up	To establish a correction factor for the calculation of hardness
Frick *et al.* (2005)	AFM	—	—	—	$d_{max} \approx 20$ mm	Commercial polycrystalline NiTi	Vickers	Recovery	To determine the indent depth before heating and after heating. Observation of the recovery ratio
Gadelrab *et al.* (2012)	AFM	—	—	—	$d_{max} \approx 40$ μm	Fused silica	Berkovich	Pile-up	To observe if pile-up occurs. Pile-up value is very close to the simulation
Göken and Kempf ('99)	AFM	—	—	—	$d_{max} \approx 0.2$ μm	CMSX-6 and Waspalloy	Berkovich	Phase	Position of indents in the phases
Hainsworth *et al.* ('98)	SEM	CamScan S4-80 DV	—	—	$d_{max} \approx 250$ μm	TiN only, NbN only and TiN/NbN multilayers and a complex multilayer of TiN/ZrN	Berkovich and Vickers	Cracks	To observe cracks
	Profilometer	Micromap 512, Burleigh instruments	—	≈0.1 Å	$d_{max} \approx 250$ μm	TiN only, NbN only and TiN/NbN multilayers and a complex multilayer of TiN/ZrN	Berkovich	Cracks	To check the length of the crack measured with the SEM
	Scanning electron acoustic microscope	Cambridge Technology	—	—	$d_{max} \approx 250$ μm	TiN only, NbN only and TiN/NbN multilayers and a complex multilayer of TiN/ZrN	Berkovich and Vickers	Cracks	To confirm the occurrence of debonding
Howell *et al.* (2008)	AFM	—	—	—	$d_{max} \approx 2$ μm	4 silicate reference glasses	Berkovich	Pile-up	To observe the evolution of pile-up as the applied force is increased
Huang *et al.* (2005)	Interferometric	WYKO	—	—	$d_{max} \approx 15$ μm	NiTi shape-memory alloy	Vickers	Pile-up	To study the relationship between temperature and pile-up
Huang *et al.* (2010)	3D NanoVision scans	NanoVision system	—	—	$d_{max} \approx 5$ μm	Ti-based bulk metallic glass	Berkovich	Pile-up	To check pile-up appearance
Jee and Lee (2010)	AFM	XE-70, PSIA	—	—	$d_{max} \approx 1$ μm	Various polymers: LDPE, PVA, HDPE, UHMWPE, PVC, PC, Nylon 6, PMMA, PS, PAA	Berkovich	Pile-up	To measure the contact area

Continued

TABLE I Continued

Refs.	Technique	Device reference	Z range	Z Resolution	Scale	Material	Indenter type	Application	Aim
Karthik *et al.* (2012)	Profilometer	Dektak 6 M	—	0.02 μm	$d_{max} \approx 0.8$ mm	AISI 316 stainless steel, low carbon steel and modified 9Cr-1Mo steel	Ball indentation (d = 1 mm)	Simulation	Comparison of the simulated profiles with the experimental ones to choose the friction coefficient of the simulation
Kashani and Madhavan (2011)	AFM	—	—	—	$d_{max} \approx 1.2$ μm	Fused quartz	Berkovich	Symmetry	To look at the indentation shape
Keryvin (2007)	Optical	Olympus BX60F-3	—	—	$d_{max} \approx 640$ μm	BMGs	Berkovich, Vickers, conical with apex angles of 90°, 136°, 148°, 120° conical with a 160 μm spherical tip and a 2.5 mm sphere	Simulation	To examine the causes of the development of shear bands
	SEM	Jeol JSM 6301 F	—	—	—	BMGs	Vickers	Simulation	To examine the causes of the development of shear bands
	Confocal	Leica ICM1000	—	—	$d_{max} \approx 20$ μm	BMGs	Vickers	Pile-up	To observe pile-up
	AFM	Nanoscope III 3100, Digital Instruments	—	—	$d_{max} \approx 20$ μm	BMGs	Vickers	Pile-up	To observe pile-up
Kese *et al.* (2005)	AFM	Dimension 3100 Series, Digital Instruments	—	—	$d_{max} \approx 5$ μm	Soda-lime glass	Berkovich	Pile-up	To observe pile-up
Lee *et al.* (2009)	AFM	—	—	—	$d_{max} \approx 6$ μm	Al6061-T6 and copper (99%)	Berkovich	Pile-up	To observe pile-up and sink-in
Liu et al. (2008)	AFM	Dimension 3100, Digital Instruments	—	—	$d_{max} \approx 3$ μm	(100), (011), and (111) single crystal copper	Spherical indenter (r = 3.4 μm)	Pile-up	Observation of the pile-up patterns and comparison with the simulation result. Measurement of the plastic zone
Marteau *et al.* (2012)	Interferometric	Zygo NewView 200	—	1 nm	$d_{max} \approx 20$ μm	316 L stainless steel	Berkovich	Pile-up	To check pile-up appearance
Mordehai *et al.* (2011)	SFM	XE-70, Park Systems Corp.	—	—	$d_{max} \approx 150$ nm	Au particles on sapphire substrates	Berkovich	Coating	To observe the topography and pile-up appearance near the indent
Navamathavan *et al.* (2006)	AFM	—	—	—	$d_{max} \approx 5$ μm	InGaAsP epilayers on InP substrate	Vickers	Symmetry	To investigate the surface topography (pile-up/sink-in/cracks) and the indentation depth
Ou *et al.* (2008)	3D NanoVision	—	—	—	d ≈ 60 μm	KMPR (photosensitive resin)	Berkovich	Pile-up	To check pile-up appearance
Randall *et al.* ('96)	SFM	—	—	—	$d_{max} \approx 300$ nm	High speed steel. MgC carbide particle. MnS grain. MC carbide particle	Vickers	Pile-up	Observation of pile-up
Santos *et al.* ('98)	Confocal	—	—	≈0.1 μm	$d_{max} \approx 35$ μm	Two tempered martensitic steels, two low alloy reactor pressure vessel steels, a low work-hardening Nb-47.5% alloy and an AISI 302 austenitic stainless steel	Vickers	Pile-up	To further examine the relationship between the work-hardening behavior and the appearance of pile-up
Schneider *et al.* ('99)	Optical or confocal	Lasertec confocal	—	—	$d_{max} \approx 50$ μm	Hardness standard	Vickers	Hardness	To study the statistical dispersion in Vickers hardness measurements
Stelmashenko *et al.* ('93)	STM	Nanoscope 2	—	—	d = 1–5 μm	(100), (110), and (111) surfaces of Mo and W single crystals	Vickers	Pile-up	To find the relationship between pile-up and the geometry of the crystal slip systems
	Optical	—	—	—	d = 10–100 μm	Mo and W crystals	Vickers	Pile-up	To find the relationship between pile-up and the geometry of the crystal slip systems
Su and Anand (2006)	Optical	—	—	—	$d_{max} \approx 0.4$ mm	Zr-based metallic glass	Triangular cutting tool with a cylindrical tip	Shear-bands	To compare the experimental shear-bands with the simulation results
Su *et al.* (2012)	Interferometric	ADE Phase Shift MicroXAM	—	—	$d_{max} \approx 80$ μm	Amorphous selenium	Berkovich	Pile-up	To check the appearance of pile-up or sink-in
Woodcock and Bahr (2000)	Scanning Probe Mode	Hysitron Triboscope	—	—	$d_{max} \approx 2$ μm	Fe-3%Si single crystal oriented in the <100> direction	Berkovich and cube corner	Hardness	To observe and measure the lobes of deformation
Yang *et al.* (2006)	Optical	—	—	—	d ≈ 25 μm	Annealed Al	Spherical indenter (radius = 0.01, 0.05, 0.1, 0.2, and 0.5 mm)	Illustration	To show residual impression
Yang *et al.* (2008)	AFM	Asylum Research	—	—	$d_{max} \approx 0.5$ μm	Shape memory polymer	AFM tip	Recovery	To measure the recovery of the material in function of the temperature
Youn and Kang (2006)	AFM	XE-100, PSIA	—	—	$d_{max} \approx 10$ μm	Squeeze-cast A356-T5 alloy	Berkovich	Hardness	To understand the difference of hardness among heat-treated squeeze-cast alloy
Zhang *et al.* (2011)	Laser confocal microscope	LEXT OLS4000	—	—	$d_{max} \approx 100$ μm	Cu and Cu-Zn alloys with different microstructures, various BMGs and ceramics.	Vickers	Pile-up	To observe the shape of the impression, pile-up and cracks

Continued

TABLE I Continued

Refs.	Technique	Device reference	Z range	Z Resolution	Scale	Material	Indenter type	Application	Aim
Zhou *et al.* (2008)	SEM	Hitachi S-3000N	—	—	$d \approx 10$ μm	Au/glass-ceramic and Al/7059 glass	Berkovich	Pile-up	To measure the residual impressions to calculate the actual contact area and amount of pile-up
	Profilometer	XP-2 stylus, Ambios	—	—	$d \approx 10$ μm	Au/glass-ceramic and Al/7059 glass	Berkovich	Pile-up	To measure the residual impressions to calculate the actual contact area and amount of pile-up
	AFM	AutoProbe system, Veeco	—	—	$d \approx 10$ μm	Au/glass-ceramic and Al/7059 glass	Berkovich	Pile-up	To measure the residual impressions to calculate the actual contact area and amount of pile-up
Zong and Soboyejo (2005)	AFM	—	—	—	$d_{max} \approx 5$ μm	Au, Ag, and Ni single crystals with (001), (011), and (111) orientations	Berkovich	Pile-up	To study pile-up shapes in function of crystal orientation and the load of appearance

Z refers to the out-of-plane displacement and d to the diagonal or bisector of the indentation imprint.

to the one proposed by Marteau *et al*. (2012) to deal with the scatter of the load-versus-indentation depth curves could be adapted to the imprint study.

All these difficulties show that there is a need for some standardization.

Conclusion and Perspectives

In this paper, three main uses of the indentation imprint were identified: the validation and the understanding of the indentation results, the material characterization, and the employment of the imprint in finite element or molecular dynamics simulation for the identification of material parameters. An overview of these different aspects is presented in Table I.

Inspection of the methods used to quantify the pile-up in the literature emphasized the lack of standardization in the measurements. No studies were made to try to identify which parameter is the most relevant to describe the indentation imprint. Similarly, there is no prevailing technique for the measurement of the imprint. Different technologies are used for the same purposes. Some of the difficulties encountered in the observation of residual indentation imprint also have been discussed. The different parts of this review clearly show that there is a need for creating standardized morphological indicators. The latter requires statistical evaluations of the imprint for different materials, which would provide more reliable experimental information for different application fields and thus widen the use of the indentation imprint.

References

Alcalá J, Casals O, Ocenásek J. 2008. Micromechanics of pyramidal indentation in FCC metals: single crystal plasticity finite element analysis. J Mech Phys Solids 56:3277–3303.

An T, Wang LL, Tian HW, Wen M, Zheng WT. 2011. Deformation and fracture of TiN coating on a Si(1 1 1) substrate during nanoindentation. Appl Surf Sci 257:7475–7480.

Arivuoli D, Lawson NS, Krier A, Attolini G, Pelosi C. 2000. Nanoindentation studies of MOVPE grown GaAs/InP heterostructures. Mater Chem Phys 66:207–212.

Arpat E, Ürgen M. 2011. Production of free standing Cu–Al intermetallics by cathodic arc plasma treatment. Intermetallics 19:1817–1822.

Babu JSS, Kang CG. 2010. Nanoindentation behaviour of aluminium based hybrid composites with graphite nanofiber/alumina short fiber. Mater Des 31:4881–4885.

Barnoush A, Welsch MT, Vehoff H. 2010. Correlation between dislocation density and pop-in phenomena in aluminum studied by nanoindentation and electron channeling contrast imaging. Scripta Mater 63:465–468.

Barshilia HC, Rajam KS. 2002. Characterization of Cu/Ni multilayer coatings by nanoindentation and atomic force microscopy. Surf Coat Technol 155:195–202.

Beegan D, Chowdhury S, Laugier MT. 2003. A nanoindentation study of copper films on oxidised silicon substrates. Surf Coat Technol 176:124–130.

Beegan D, Chowdhury S, Laugier MT. 2004. The nanoindentation behaviour of hard and soft films on silicon substrates. Thin Solid Films 466:167–174.
Beegan D, Chowdhury S, Laugier MT. 2005. Work of indentation methods for determining copper film hardness. Surf Coat Technol 192:57–63.
Bellemare S, Dao M, Suresh S. 2007. The frictional sliding response of elasto-plastic materials in contact with a conical indenter. Int J Solids Struct 44:1970–1989.
Bertoldi M, Sglavo VM. 2004. Soda–borosilicate glass: normal or anomalous behavior under Vickers indentation? J Non-Cryst Solids 344:51–59.
Bhattacharya S, Riahi AR, Alpas AT. 2009. Indentation-induced subsurface damage in silicon particles of Al–Si alloys. Mater Sci Eng A 527:387–396.
Blunt L, Sullivan PJ. 1994. The measurement of the pile-up topography of hardness indentations. Tribol Int 27:69–79.
Bolelli G, Cannillo V, Lusvarghi L, et al. 2008. An FIB study of sharp indentation testing on plasma-sprayed TiO2. Mater Lett 62:1557–1560.
Bolzon G, Maier G, Panico M. 2004. Material model calibration by indentation, imprint mapping and inverse analysis. Int J Solids Struct 41:2957–2975.
Brown CA, Siegmann S. 2001. Fundamental scales of adhesion and area—scale fractal analysis. Int J Mach Tools Manuf 41:1927–1933.
Cabibbo M, Ricci P. 2013. True hardness evaluation of bulk metallic materials in the presence of pile up: analytical and enhanced lobes method approaches. Metall Mater Trans A 44:1–13.
Cantor GJ, Brown CA. 2009. Scale-based correlations of relative areas with fracture of chocolate. Wear 266:609–612.
Carvalho NJM, De Hosson JTM. 2006. Deformation mechanisms in TiN/(Ti,Al)N multilayers under depth-sensing indentation. Acta Mater 54:1857–1862.
Casals O, Alcalá J. 2005. The duality in mechanical property extractions from Vickers and Berkovich instrumented indentation experiments. Acta Mater 53:3545–3561.
Charleux L, Gravier S, Verdier M, Fivel M, Blandin JJ. 2008. Amorphous and partially crystallized metallic glasses: an indentation study. Mater Sci Eng A 483–484:652–655.
Chaudhri MM, Winter M. 1988. The load-bearing area of a hardness indentation. J Phys D Appl Phys 21:370–374.
Chen X, Ogasawara N, Zhao M, Chiba N. 2007. On the uniqueness of measuring elastoplastic properties from indentation: the indistinguishable mystical materials. J Mech Phys Solids 55:1618–1660.
Chen K-W, Jian S-R, Wei P-J, Jang JSC, Lin J-F. 2010. A study of the relationship between semi-circular shear bands and pop-ins induced by indentation in bulk metallic glasses. Intermetallics 18:1572–1578.
Chen L, Yeap KB, She CM, Liu GR. 2011. A computational and experimental investigation of three-dimensional micro-wedge indentation-induced interfacial delamination in a soft-film-on-hard-substrate system. Eng Struct 33:3269–3278.
Choi IS, Detor AJ, Schwaiger R, et al. 2008. Mechanics of indentation of plastically graded materials–II: experiments on nanocrystalline alloys with grain size gradients. J Mech Phys Solids 56:172–183.
Constantinides G, Ravi Chandran KS, Ulm FJ, Van Vliet KJ. 2006. Grid indentation analysis of composite microstructure and mechanics: principles and validation. Mater Sci Eng A 430:189–202.
Das G, Ghosh S, Ghosh S, Ghosh RN. 2005. Materials characterization and classification on the basis of materials pile-up surrounding the indentation. Mater Sci Eng A 408:158–164.
Demir E, Raabe D, Zaafarani N, Zaefferer S. 2009. Investigation of the indentation size effect through the measurement of the geometrically necessary dislocations beneath small indents of different depths using EBSD tomography. Acta Mater 57:559–569.
Dwyer-Joyce SR, Ushijima Y, Murakami Y, Shibuta R. 1998. Some experiments on the micro-indentation of digital audio tape. Tribol Int 31:525–530.
Eidel B. 2011. Crystal plasticity finite-element analysis versus experimental results of pyramidal indentation into (0 0 1) fcc single crystal. Acta Mater 59:1761–1771.
Elban WL, Armstrong RW. 1998. Plastic anisotropy and cracking at hardness impressions in single crystal ammonium perchlorate. Acta Mater 46:6041–6052.
Farges G, Degout D. 1989. Interpretation of the indentation size effect in Vickers microhardness measurements-absolute hardness of materials. Thin Solid Films 181:365–374.
Fischer-Cripps AC. 2006. Critical review of analysis and interpretation of nanoindentation test data. Surf Coat Technol 200:4153–4165.
Frick CP, Ortega AM, Tyber J, et al. 2005. Thermal processing of polycrystalline NiTi shape memory alloys. Mater Sci Eng A 405:34–49.
Gadelrab KR, Bonilla FA, Chiesa M. 2012. Densification modeling of fused silica under nanoindentation. J Non-Cryst Solids 358:392–398.
Giannakopoulos AE, Larsson PL, Vestergaard R. 1994. Analysis of Vickers indentation. Int J Solids Struct 31:2679–2708.
Göken M, Kempf M. 1999. Microstructural properties of superalloys investigated by nanoindentations in an atomic force microscope. Acta Mater 47:1043–1052.
Hainsworth SV, McGurk MR, Page TF. 1998. The effect of coating cracking on the indentation response of thin hard-coated systems. Surf Coat Technol 102:97–107.
Howell JA, Hellmann JR, Muhlstein CL. 2008. Correlations between free volume and pile-up behavior in nanoindentation reference glasses. Mater Lett 62:2140–2142.
Huang WM, Su JF, Hong MH, Yang B. 2005. Pile-up and sink-in in micro-indentation of a NiTi shape-memory alloy. Scripta Mater 53:1055–1057.
Huang Y, Shen J, Sun Y, Sun J. 2010. Indentation size effect of hardness of metallic glasses. Mater Des 31:1563–1566.
Jee A-Y, Lee M. 2010. Comparative analysis on the nano-indentation of polymers using atomic force microscopy. Polym Test 29:95–99.
Karthik V, Visweswaran P, Bhushan A, et al. 2012. Finite element analysis of spherical indentation to study pile-up/sink-in phenomena in steels and experimental validation. Int J Mech Sci 54:74–83.
Kashani MS, Madhavan V. 2011. Analysis and correction of the effect of sample tilt on results of nanoindentation. Acta Mater 59:883–895.
Keryvin V. 2007. Indentation of bulk metallic glasses: relationships between shear bands observed around the prints and hardness. Acta Mater 55:2565–2578.
Kese KO, Li ZC, Bergman B. 2005. Method to account for true contact area in soda-lime glass during nanoindentation with the Berkovich tip. Mater Sci Eng A 404:1–8.
Lee J, Lee C, Kim B. 2009. Reverse analysis of nano-indentation using different representative strains and residual indentation profiles. Mater Des 30:3395–3404.
Liu Y, Varghese S, Ma J, et al. 2008. Orientation effects in nanoindentation of single crystal copper. Int J Plast 24:1990–2015.
Marteau J, Mazeran PE, Bouvier S, Bigerelle M. 2012. Zero-point correction method for nanoindentation tests to accurately quantify hardness and indentation size effect. Strain 48: 491–497.
Marteau J, Bigerelle M, Xia Y, Mazeran PE, Bouvier S. 2013. Quantification of first contact detection errors on hardness and indentation size effect measurements. Tribol Int 59: 154–162.
Mordehai D, Kazakevich M, Srolovitz DJ, Rabkin E. 2011. Nanoindentation size effect in single-crystal nanoparticles

and thin films: a comparative experimental and simulation study. Acta Mater 59:2309–2321.
Navamathavan R, Ganesan V, Arivuoli D, et al. 2006. Characterization of surface deformation around Vickers indentations in InGaAsP epilayers on InP substrate. Appl Surf Sci 253:2973–2977.
Oliver WC, Pharr GM. 1992. An improved technique for determining hardness and elastic modulus using load and displacement sensing indentation experiments. J Mater Res 7: 1564–1583.
Ou KS, Yan HY, Chen KS. 2008. Mechanical characterization of KMPR by nano-indentation for MEMS applications. Strain 44:267–271.
Randall NX, Christoph R, Droz S, Julia-Schmutz C. 1996. Localised micro-hardness measurements with a combined scanning force microscope/nanoindentation system. Thin Solid Films 290–291:348–354.
Santos C, Odette GR, Lucas GE, Yamamoto T. 1998. Examination of indention geometry-constitutive behaviour relations with confocal microscopy and finite element modeling. J Nucl Mater 258–263(Part 1):452–456.
Schneider JM, Bigerelle M, Iost A. 1999. Statistical analysis of the Vickers hardness. Mater Sci Eng A 262:256–263.
Stelmashenko NA, Walls MG, Brown LM, Milman YV. 1993. Microindentations on W and Mo oriented single crystals: an STM study. Acta Metall Mater 41:2855–2865.
Su C, Anand L. 2006. Plane strain indentation of a Zr-based metallic glass: experiments and numerical simulation. Acta Mater 54:179–189.
Su C, Herbert EG, Sohn S, et al. 2012. Measurement of power-law creep parameters by instrumented indentation methods. J Mech Phys Solids 61:517–536.
Wang C-T, Jian S-R, Jang JS-C, Lai Y-S, Yang P-F. 2008. Multiscale simulation of nanoindentation on Ni (1 0 0) thin film. Appl Surf Sci 255(5 Part 2):3240–3250.
Woodcock CL, Bahr DF. 2000. Plastic zone evolution around small scale indentations. Scripta Mater 43:783–788.
Yang F, Peng L, Okazaki K. 2006. Effect of the indenter size on the indentation of aluminum. Mater Charact 57:321–325.
Yang F, Wornyo E, Gall K, King WP. 2008. Thermomechanical formation and recovery of nanoindents in a shape memory polymer studied using a heated tip. Scanning 30:197–202.
Youn SW, Kang CG. 2006. Characterization of age-hardening behavior of eutectic region in squeeze-cast A356-T5 alloy using nanoindenter and atomic force microscope. Mater Sci Eng A 425:28–35.
Zhang P, Li SX, Zhang ZF. 2011. General relationship between strength and hardness. Mater Sci Eng A 529:62–73.
Zhou X, Jiang Z, Wang H, Yu R. 2008. Investigation on methods for dealing with pile-up errors in evaluating the mechanical properties of thin metal films at sub-micron scale on hard substrates by nanoindentation technique. Mater Sci Eng A 488:318–332.
Zong Z, Soboyejo W. 2005. Indentation size effects in face centered cubic single crystal thin films. Mater Sci Eng A 404:281–290.